Nano Research 2014, 7(4): 502–510
DOI 10.1007/s12274-014-0416-0
Research Article

ISSN 1998-0124
CN 11-5974/O4

Preparation of carbon-coated iron oxide nanoparticles dispersed on graphene sheets and applications as advanced anode materials for lithium-ion batteries

Huilong Fei[1,§], Zhiwei Peng[1,§], Lei Li[1], Yang Yang[1,2], Wei Lu[1], Errol L. G. Samuel[1], Xiujun Fan[1], and James M. Tour[1,2,3] (✉)

[1] *Department of Chemistry, Rice University, 6100 Main Street, Houston, Texas 77005, USA*
[2] *Richard E. Smalley Institute for Nanoscale Science and Technology, Rice University, 6100 Main Street, Houston, Texas 77005, USA*
[3] *Department of Materials Science and NanoEngineering, Rice University, 6100 Main Street, Houston, Texas 77005, USA*
[§] *These authors contribute equally to this work.*

Received: 19 November 2013
Revised: 8 January 2014
Accepted: 13 January 2014

KEYWORDS

Fe_2O_3 nanoparticles,
carbon coating,
graphene,
chemical vapor deposition (CVD),
anode,
lithium ion batteries

ABSTRACT

We report a novel chemical vapor deposition (CVD) based strategy to synthesize carbon-coated Fe_2O_3 nanoparticles dispersed on graphene sheets (Fe_2O_3@C@G). Graphene sheets with high surface area and aspect ratio are chosen as space restrictor to prevent the sintering and aggregation of nanoparticles during high temperature treatments (800 °C). In the resulting nanocomposite, each individual Fe_2O_3 nanoparticle (5 to 20 nm in diameter) is uniformly coated with a continuous and thin (two to five layers) graphitic carbon shell. Further, the core–shell nanoparticles are evenly distributed on graphene sheets. When used as anode materials for lithium ion batteries, the conductive-additive-free Fe_2O_3@C@G electrode shows outstanding Li^+ storage properties with large reversible specific capacity (864 mAh/g after 100 cycles), excellent cyclic stability (120% retention after 100 cycles at 100 mA/g), high Coulombic efficiency (~99%), and good rate capability.

1 Introduction

Rechargeable lithium ion batteries (LIBs) are attractive sustainable energy storage devices that are environmentally friendly with high output voltage and energy. LIBs with high energy/power density and long cycle life are desirable for applications in portable devices and plug-in hybrid electric vehicles [1, 2]. Conventional LIBs use graphite as the anode material, which has good cycle stability but a limited theoretical specific capacity of 372 mAh/g. By comparison, transition metal oxides, such as Fe_2O_3 [3], Fe_3O_4 [4], Co_3O_4 [5], CoO [6], MnO [7], and NiO [8], have been proven to be effective in Li^+ storage with much larger

Address correspondence to tour@rice.edu

specific capacities. In particular, Fe_2O_3 has a theoretical specific capacity of 1,005 mAh/g which, combined with its low cost, abundance and low toxicity, makes Fe_2O_3 attractive to store Li^+ as anode material [3, 9]. However, Fe_2O_3 stores Li^+ using the so-called reconstitution reaction, during which Fe_2O_3 is decomposed and reformed repeatedly during charge–discharge operations [10]. This process involves drastic volume changes, which would cause fragmentation of the anode and the destruction of the solid electrolyte interface (SEI) film, leading to fast decay of specific capacity [11, 12]. Besides its poor cycle stability, another challenge for Fe_2O_3 to be used as an anode material is its limited rate capability that results from its low electrical and ionic conductivity [13].

To overcome these problems, decreasing the particle size to the nano-range and coating the particles with conductive carbon shells improves the stability and kinetics of the Fe_2O_3 electrode. The capacity-fading problem was partially resolved by the use of nanoparticles because of their better accommodation of the strain from volume expansion [14], and the rate capability was improved due to the shorter path length for electrons and Li^+ in nanoparticles than in bulk material [15]. However, the high surface area of nanoparticles means larger contact area between the electrode and electrolyte, which would lead to larger irreversible capacity and thus lower Coulombic efficiency due to the increased amounts of unstable SEI [16, 17]. The use of the carbon coating stabilizes the SEI by avoiding direct contact of the metal oxide nanoparticles with the electrolyte [18]. In addition, the carbon coating further improves cycle stability by lowering the volume change during charge–discharge operations and prevents some side reactions between electrode and electrolyte [19, 20]. The rate capability can be further improved by the enhanced electrical conductivity due to the carbon coating [14, 20].

With the realization of the merits of nano-sized materials with carbon coatings, carbon-coated iron oxide (Fe_2O_3 or Fe_3O_4) nanospheres [21], nanorods [12, 22], nanospindles [14] and nanowires [23] have been prepared and they exhibited improved electrochemical performance when used as anode materials for LIBs. However, the carbon coatings to date were of low quality, primarily in an amorphous form, as the growth temperatures were intentionally kept low, at 400 to 600 °C, compared to the high temperature required to obtain graphitic carbon without using metallic catalysts [24, 25]. Low temperatures also prevent the aggregation of nanoparticles as well as the reduction of iron oxide to metallic iron through a carbothermal reduction process [26]. As a result, the cycle stability and rate capability of these materials demonstrated limited improvement. In this paper, we report the design and synthesis of iron oxide nanoparticles (5 to 20 nm in diameter) coated with uniform and thin graphitized carbon shells (two to five layers) well dispersed on graphene sheets. Benefiting from the protective and conductive graphitized carbon shells and graphene sheets, this nanocomposite displays superior electrochemical performance in Li^+ storage with excellent cycle stability, rate capability, large specific capacity and high Coulombic efficiency.

2 Results and discussion

The preparation of Fe_2O_3@C@G is illustrated in Fig. 1. We started with a nanocomposite of magnetite nanoparticles on graphene sheets (Fe_3O_4@G). The Fe_3O_4 nanoparticles were synthesized according to an established protocol [27] in the presence of graphene oxide (GO) (see the Electronic Supplementary Material (ESM) for details). The GO oxygen functional groups facilitate the nucleation and growth of Fe_3O_4 nanoparticles. Transmission electron microscopy (TEM) images (Fig. S1 in the ESM) show that the Fe_3O_4 nanoparticles, with diameters < 10 nm, were evenly anchored on the GO. The resulting Fe_3O_4@G was then placed in a chemical vapor deposition (CVD) furnace to grow the carbon coating using a two-step synthesis procedure, during which the GO was converted to graphene. In the first step, the Fe_3O_4 nanoparticles were reduced in a H_2 atmosphere at 450 °C to metallic Fe nanoparticles, which then acted as catalysts for the growth of graphitic carbon in the following step. Second, semipermeable graphitized carbon shells were grown around the Fe nanoparticles using CH_4 as a carbon source at 800 °C to obtain carbon-coated Fe on graphene (Fe@C@G). Finally, Fe in the core structure was oxidized in air at 280 °C to Fe_2O_3 to obtain the final product Fe_2O_3@C@G. The graphitic

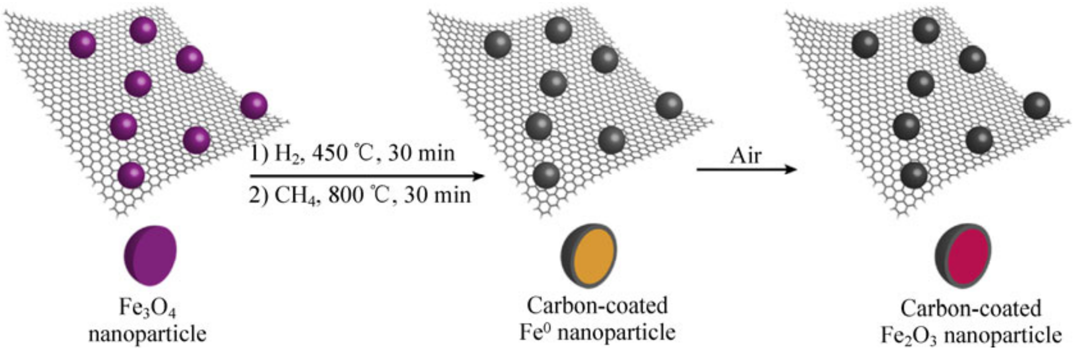

Figure 1 Illustration of the synthesis of the Fe_2O_3@C@G nanocomposite via a two-step CVD reduction and carbon growth followed by air oxidation.

carbon coating was rendered more permeable during this process due to expansion upon oxidation.

Figure 2 shows scanning electron microscopy (SEM) and TEM images of the Fe@C@G nanocomposite. From the SEM image (Fig. 2(a)), small nanoparticles were closely and evenly packed on the surface of the graphene sheets. The low magnification TEM image (Fig. 2(b)) shows individual graphene sheets homogenously decorated with nanoparticles 5 to 20 nm in diameter. The small size and uniformity of these nanoparticles was maintained after the 800 °C treatment; apparently the strong interaction between the graphene sheets and the nanoparticles prevented their aggregation. From the high resolution TEM images (Figs. 2(c) and 2(d)), it can be seen that the nanoparticles are uniformly coated with thin graphitized carbon shells with a thickness of two to five layers. The CVD method is known to produce a uniform and complete carbon coating, making it a coating technique superior to others such as ball milling [28], wet mixing [29], and hydrothermal treatment [30, 31]. From the high resolution TEM image in Fig. 2(d), the core structure is crystalline and the lattice fringes with an interlayer distance of 0.201 nm correspond to the spacing between (110) planes of α-Fe crystals. The X-ray diffraction patterns (XRD) (Fig. S2 in the ESM) show the peaks characteristic of α-Fe (JCPDS 89-7194) with the coexistence of peaks for Fe_3C (JCPDS 03-1055) and graphite (JCPDS 12-0212).

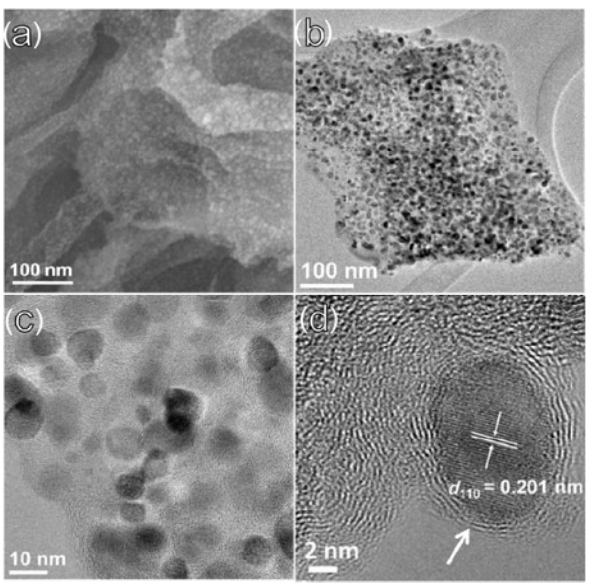

Figure 2 (a) SEM image of Fe@C@G. (b)–(d) TEM images of Fe@C@G at different magnifications. (d) Shows the Fe^0 lattice fringes with the surrounding graphene shells (indicated by arrow).

Fe@C@G was then subjected to air oxidation to convert Fe to Fe_2O_3, which was then used as the active material for Li^+ storage in the assembled LIB device. Figures 3(a) and 3(b) show the low and high resolution TEM images of Fe_2O_3@C@G. It can be seen that the morphology of the sheet-like structure of Fe_2O_3@C@G is quite similar to Fe@C@G, but with less contrast due to the lower electrical conductivity of Fe_2O_3. The images show that the carbon shells were well preserved after air oxidation. Any cracking of the thin carbon shells because of nanoparticle expansion during the oxidation may enable the transport of Li^+ through the carbon shells. Interestingly, apart from the solid core–shell structure, we also observed some nanoparticles with yolk–shell structure (Fig. S3 in the ESM), which can be explained by a nanoscale

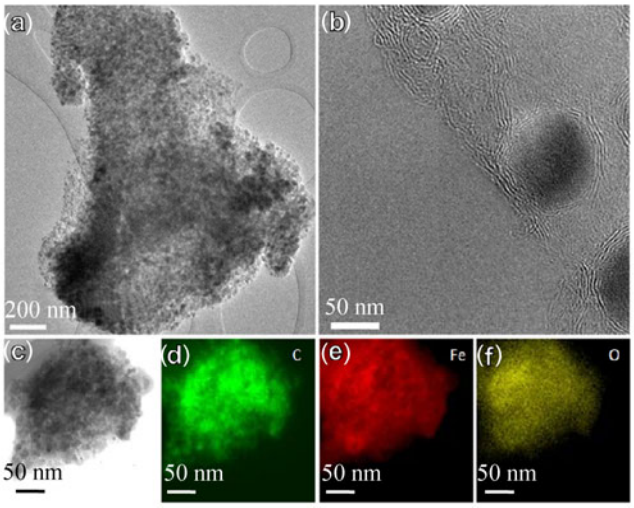

Figure 3 (a) Low and (b) high magnifications TEM images of Fe_2O_3@C@G. (c) Energy filter transmission electron microscopy (EFTEM) image and corresponding elemental mapping images of (d) carbon (e) iron and (f) oxygen, showing the homogeneous dispersion of iron and oxygen on the graphene sheets.

Kirkendall effect during the oxidation reaction [32]. The elemental mapping analysis (Figs. 3(c)–3(f)) shows a uniform distribution of C, Fe, and O.

X-ray photoelectron spectroscopy (XPS) was used to determine the chemical composition of the Fe_2O_3@C@G nanocomposite. The survey spectrum (Fig. 4(a)) shows peaks characteristic of Fe, O, and C. The Fe2p spectrum (Fig. 4(b), red curve), which is sensitive to the valence state of iron, shows that the peaks for $Fe2p_{3/2}$ and $Fe2p_{1/2}$ from Fe_2O_3@C@G are at 710.7 eV and 724.2 eV (compared to 707.0 eV and 720.3 eV for metallic Fe in the Fe@C@G composite before the air oxidation treatment, as shown in the black curve in Fig. 4(b)), consistent with Fe_2O_3 [33]. In addition, the presence of the satellite peak in Fe_2O_3@C@G is characteristic of Fe^{3+} in Fe_2O_3 [34]. The iron oxide formed here was identified to be the hematite phase, α-Fe_2O_3 (see the XRD pattern in Fig. S4 in the ESM). The absence of peaks representing metallic Fe and Fe_3C in the XRD pattern, combined with the Fe2p XPS spectra discussed above, indicates the successful conversion of Fe to Fe_2O_3 by air oxidation. The specific surface area and pore size distribution of Fe_2O_3@C@G were analyzed using nitrogen adsorption measurements. The adsorption–desorption isotherm and pore size distributions are shown in Fig. S5 (in the ESM). The Brunauer–Emmett–Teller (BET) surface area of Fe_2O_3@C@G was calculated to be 156 m^2/g, which is higher than the surface areas for other reported iron oxide carbon composites (< 120 m^2/g) [14, 18, 35] and mesoporous iron oxides (116–128 m^2/g) [36, 37]. This higher surface area should facilitate the surface electrochemical reaction. The pore size distribution curve plotted from the desorption isotherm using the Barrett–Joyner–Halenda (BJH) method revealed the presence of pores of size ~38 nm. The pore size measurement was made on the Fe_2O_3@C@G composite and is therefore a combination of the space between the nanoparticles and between the nanoparticles and graphene sheets. It is reasonable that the measured pore size is larger than the Fe_2O_3@C nanoparticles (Fig. 2(b)). The Fe_2O_3 content was determined to be ~78 wt.% in the nanocomposite by thermal gravimetric analysis (TGA) performed in air (Fig. S6 in the ESM).

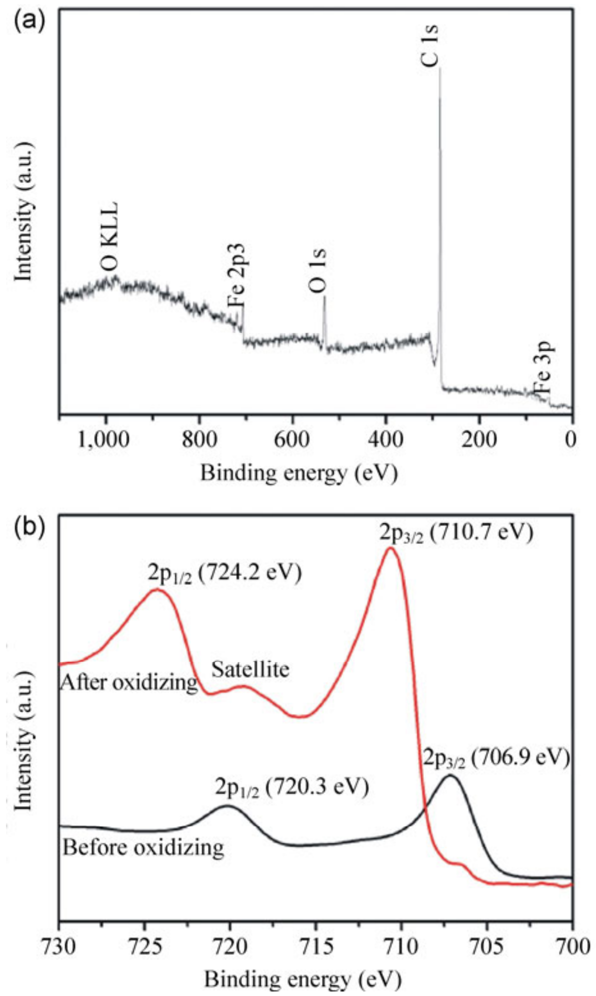

Figure 4 (a) XPS survey spectrum of Fe_2O_3@C@G. (b) Fe2p spectrum of Fe@C@G (black curve) and Fe_2O_3@C@G (red curve).

To test the electrochemical performance of the composite when used as an anode in a LIB, coin cells were fabricated using metallic lithium foil as the counter electrode; the working electrode was prepared by mixing the composite with poly(vinylidene difluoride) (PVDF) at a weight ratio of 90:10. In contrast to other studies [14, 18, 22, 38], no other conductive additives were added since we expected good electrical conductivity from the graphene sheets and graphitized carbon shells. The lack of additional conductive materials has a crucial practical implication since the additional weight of an additive would lower the specific capacity of the electrode. Figure 5(a) shows cyclic voltammograms of a Fe_2O_3@C@G electrode at a scan rate of 0.2 mV/s for the first two cycles. In the cathodic process of the first cycle, a broad peak is observed at ~0.5 V, which can be attributed to the combined processes of lithium intercalation, reductive reaction of Fe^{3+} to Fe^{2+}/Fe^0 and irreversible reaction with electrolyte. In the anodic scan, a main peak at ~1.7 V is observed and can be ascribed to the oxidative reactions of Fe^0 to Fe^{2+} and Fe^{3+}. In the 2nd cycle, the cathodic peak becomes much sharper and shifts positively to ~1.3 V compared to the 1st cycle, while the position of the anodic peak remains almost unchanged. Figure 5(b) shows the galvanostatic charge–discharge profiles for the 1st and 2nd cycles at a current density of 100 mA/g in the voltage range from 0.01 to 3 V. The 1st discharge curve consists of two slope regions and a plateau. The first slope from 1.5 to 0.8 V is attributed to the Li^+ insertion into the iron oxide lattice accompanied by a reduction from Fe^{3+} to Fe^{2+} [33]. The plateau at ~0.8 V is due to the further conversion of Fe^{2+} to metallic Fe^0 [39]. The second slope after 0.8 V is due to the reversible Li^+ storage in the graphene sheets and the decomposition of the electrolyte. The 1st discharge and charge specific capacities were found to be 1,038 mAh/g and 891 mAh/g, respectively, and this gives a 1st cycle Coulombic efficiency of 86%. The irreversible 14% capacity loss is mainly due to the electrolyte decomposition and the formation of the SEI [10, 40, 41]. The 1st cycle Coulombic efficiency

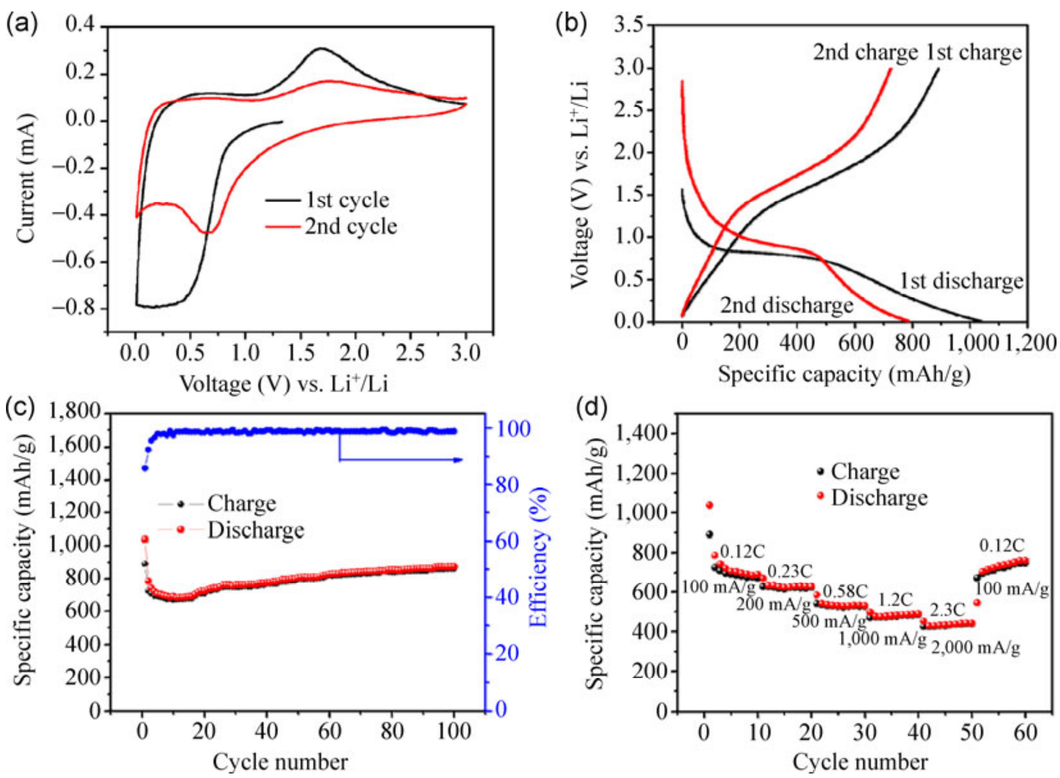

Figure 5 (a) Cyclic voltammograms of Fe_2O_3@C@G electrode at a scan rate of 0.2 mV/s for the first two cycles. (b) Galvanostatic charge–discharge profiles of the first two cycles of Fe_2O_3@C@G at a current density of 100 mA/g and a voltage range of 0.01 to 3 V. (c) The cycle performance of Fe_2O_3@C@G at a current density of 100 mA/g. (d) Rate performance of Fe_2O_3@C@G at five different current densities.

is higher than those reported for carbon coated CNT@Fe_2O_3 (55%) [42], polypyrrole-coated Fe_2O_3@C (70%) [11], Fe_3O_4/C core–shell nanorods (71.7%) [22] or carbon coated Fe_3O_4 nanospindles (80%) [14]. The reduced irreversible capacity of Fe_2O_3@C@G compared to these composites can be ascribed to the complete carbon coating of the Fe_2O_3, which apparently prevents direct contact of the electrolyte with the iron oxide nanoparticles and stabilizes the SEI formed on the interface [19, 38]. The increased Coulombic efficiency is critical in practical applications, as lower Coulombic efficiency correlates to loss of Li^+ from the cathode material, which would add weight to a fully configured battery [43]. From the 2nd cycle onwards (Fig. 5(c)), the discharge capacity slightly decreased from 726 mAh/g to 673 mAh/g after the following 10 cycles and then gradually increased to 864 mAh/g after 100 cycles, corresponding to a 20% increase compared to the discharge capacity at the 2nd cycle. The specific capacity increase may be due to the formation of a gel-like layer or an activation process to allow the full utilization of the well-coated iron oxide nanoparticles [10, 44]. The Coulombic efficiency remained near 99% after 10 cycles, indicative of the stability of the SEI film and good reversibility of the electrochemical reactions [11, 45]. The morphology of the Fe_2O_3@C@G electrode after 100 cycles was further examined by TEM and it can be seen from Fig. 6(a) and Fig. S10 (in the ESM) that the nanoparticles were still well encapsulated in the carbon shells, which helps explain the good cycle stability of Fe_2O_3@C@G electrode. To explore the long-term cycle stability at a high charge–discharge rate, the Fe_2O_3@C@G electrode was first cycled five times at a current density of 100 mA/g and then cycled up to 300 times at a relatively high current density of 2,000 mA/g. It can be seen from Fig. S7 (in the ESM) that after 350 cycles at this high rate, the specific capacity remained at ~405 mAh/g, which is above the theoretical specific capacity of graphite (372 mAh/g), the most commonly used commercial anode material. For comparison, the cycle test was also performed on bare Fe_3O_4 nanoparticles, which were synthesized using the same synthesis method, however, they had no GO or carbon coatings. The charge–discharge profiles for the first two cycles and the 100 cycle performance at a current density of 100 mA/g for the control Fe_3O_4 electrode are shown in Fig. S8 (in the ESM). The control Fe_3O_4 electrode had 1st discharge and charge capacities of 1,522 mAh/g and 1,010 mAh/g, respectively, producing a much lower first cycle Coulombic efficiency of 66%. After ten cycles, it suffered a sharp capacity decay with a negligible specific capacity of ~30 mAh/g remaining. This indicates that the cycle performance of the Fe_2O_3@C@G electrode was greatly improved by the uniform distribution of Fe_2O_3 on graphene sheets and the graphitized carbon coating around the Fe_2O_3 nanoparticles.

In addition to its superior cycle performance, the Fe_2O_3@C@G electrode also shows excellent rate capability. The rate capability was evaluated by cycling the electrode 10 times each at five different current densities; the results are shown in Fig. 5(d) and Fig. S9 (in the ESM). At discharging current densities as high as 1,000 mA/g (corresponding to 1.2 C) and 2,000 mA/g (2.3 C), the specific capacities remained at 480 mAh/g and 430 mAh/g, corresponding to 67% and 60% retention compared to 100 mA/g. In addition, when the current density was reduced back to the initial 100 mA/g, the specific capacity recovered to ~750 mAh/g, indicating that the structure of the electrode remained stable even after the high rate cycling. To reveal the good conductivity of Fe_2O_3@C@G electrode, electrochemical impedance spectra (EIS) was performed after two cycles of charge–discharge at 100 mA/g and the resulted Nyquist plots of the Fe_2O_3@C@G electrode and control Fe_3O_4 electrode are compared in Fig. 6(b). It reveals that the Fe_2O_3@C@G electrode has a much lower charge transfer resistance

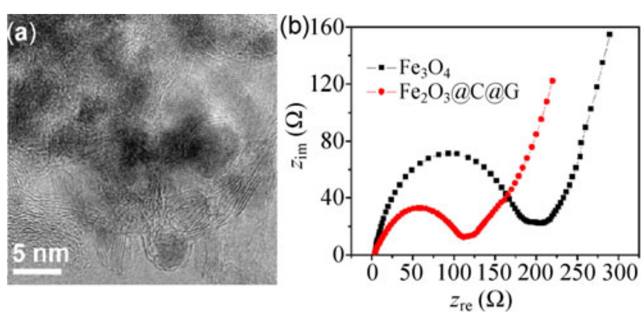

Figure 6 (a) TEM image of Fe_2O_3@C@G electrode after 100 cycles at 100 mA/g. (b) Nyquist plots of ac impedance spectra in the frequency range between 100 kHz and 10 mHz.

than that of Fe_3O_4 (~105 vs. ~190 Ω), indicating faster Li^+ diffusion and electron transfer in Fe_2O_3@C@G electrode.

The high Coulombic efficiency, cycle stability and rate capability of Fe_2O_3@C@G can be attributed to the following factors: 1) The small size of the iron oxide nanoparticles that allows fast transport of electrons and Li^+ ions; the large surface area provides an efficient interface for the electrochemical reaction; 2) the electrical conductivity of the composite is greatly improved by the hierarchically conductive network resulting from the uniform and continuous graphitized carbon coating as well as from the graphene sheets, which act as nano-current collectors to electrically interconnect the physically isolated iron oxide nanoparticles with conductive carbon shells; 3) the carbon coating shells and graphene sheets improve the structural integrity and robustness of the electrode by suppressing sintering and volume change during cycling. In addition, they presumably prevent direct contact between the iron oxide nanoparticles and electrolyte during cycling, thus decreasing the irreversible capacity coming from the formation and propagation of an unstable SEI.

3 Conclusion

In summary, we have successfully developed a strategy to coat Fe_2O_3 with a uniform and thin graphitized carbon shell using a CVD-based method; graphene sheets were added as space restrictors to prevent high temperature aggregation of nanoparticles. The resulting Fe_2O_3 nanoparticles in the Fe_2O_3@C@G nanocomposite are 5 to 20 nm in size and are encapsulated with thin graphitized carbon shells (two to five layers). In addition, these Fe_2O_3 nanoparticles with core–shell structure are evenly distributed on two-dimensional graphene sheets, which act as nano-current collectors to electrically interconnect the physically separated Fe_2O_3 nanoparticles. In this unique architecture, the carbon shells and graphene sheets provide electrical networks to allow fast and efficient electron transport, they strengthen the structural integrity and robustness of the electrode and they suppress the aggregation/sintering of the electrode. The carbon coatings on each individual Fe_2O_3 nanoparticle prevent the direct contact of electrode and electrolyte. As a result, the conductive additive-free Fe_2O_3@C@G electrode shows outstanding Li^+ storage properties with large reversible specific capacity (~864 mAh/g) after 100 cycles at a current density of 100 mA/g, excellent cyclic stability (~120% retention after 100 cycles at 100 mA/g), high Coulombic efficiency (~99%), and good rate capability. This effective strategy can be extended to construct other hybrid architectures of nano-carbon (e.g., graphene, graphene nanoribbons, carbon nanotubes) and metal oxides toward high-performance metal oxide-based anode material for LIB and other energy storage devices.

Acknowledgements

Support came from the Office of Naval Research (ONR) Multidisciplinary University Research Initiative (MURI) program (Nos. #00006766 and N00014-09-1-1066), the Air Force Office of Scientific Research (No. FA9550-09-1-0581), the Air Force Office of Scientific Research (AFOSR) Multidisciplinary University Research Initiative (MURI) program (No. FA9550-12-1-0035), and China Scholarship Council.

Electronic Supplementary Material: Supplementary material (detailed experiment procedures, morphology characterization, X-ray diffraction patterns, surface area measurements and additional electrochemical measurements) is available in the online version of this article at http://dx.doi.org/10.1007/s12274-014-0416-0.

References

[1] Armand, M.; Tarascon, J. M. Building better batteries. *Nature* **2008**, *451*, 652–657.

[2] Scrosati, B. Challenge of portable power. *Nature* **1995**, *373*, 557–558.

[3] Reddy, M. V.; Yu, T.; Sow, C. H.; Shen, Z. X.; Lim, C. T.; Subba Rao, G. V.; Chowdari, B. V. R. α-Fe_2O_3 nanoflakes as an anode material for Li-ion batteries. *Adv. Funct. Mater.* **2007**, *17*, 2792–2799.

[4] Jia, X.; Chen, Z.; Cui, X.; Peng, Y.; Wang, X.; Wang, G.; Wei, F.; Lu, Y. Building robust architectures of carbon and metal oxide nanocrystals toward high-performance anodes

for lithium-ion batteries. *ACS Nano* **2012**, *6*, 9911–9919.

[5] Poizot, P.; Laruelle, S.; Grugeon, S.; Dupont, L.; Tarascon, J. M. Nano-sized transition-metal oxides as negative-electrode materials for lithium-ion batteries. *Nature* **2000**, *407*, 496–499.

[6] Peng, C.; Chen, B.; Qin, Y.; Yang, S.; Li, C.; Zuo, Y.; Liu, S.; Yang, J. Facile ultrasonic synthesis of CoO quantum dot/graphene nanosheet composites with high lithium storage capacity. *ACS Nano* **2012**, *6*, 1074–1081.

[7] Yu, A.; Park, H. W.; Davies, A.; Higgins, D. C.; Chen, Z.; Xiao, X. Free-standing layer-by-layer hybrid thin film of graphene-MnO_2 nanotube as anode for lithium ion batteries. *J. Phys. Chem. Lett.* **2011**, *2*, 1855–1860.

[8] Needham, S. A.; Wang, G. X.; Liu, H. K. Synthesis of NiO nanotubes for use as negative electrodes in lithium ion batteries. *J. Power Sources* **2006**, *159*, 254–257.

[9] Zhu, X.; Zhu, Y.; Murali, S.; Stoller, M. D.; Ruoff, R. S. Nanostructured reduced graphene oxide/Fe_2O_3 composite as a high-performance anode material for lithium ion batteries. *ACS Nano* **2011**, *5*, 3333–3338.

[10] Xu, X.; Cao, R.; Jeong, S.; Cho, J. Spindle-like mesoporous α-Fe_2O_3 anode material prepared from MOF template for high-rate lithium batteries. *Nano Lett.* **2012**, *12*, 4988–4991.

[11] Han, F.; Li, D.; Li, W.; Lei, C.; Sun, Q.; Lu, A. Nanoengineered polypyrrole-coated Fe_2O_3@C multifunctional composites with an improved cycle stability as lithium-ion anodes. *Adv. Funct. Mater.* **2012**, *23*, 1692–1697.

[12] Yuan, S. M.; Li, J. X.; Yang, L. T.; Su, L. W.; Liu, L.; Zhou, Z. Preparation and lithium storage performances of mesoporous Fe_3O_4@C microcapsules. *ACS Appl. Mater. Inter.* **2011**, *3*, 705–709.

[13] Yu, W.; Hou, P.; Zhang, L.; Li, F.; Liu, C.; Cheng, H. Preparation and electrochemical property of Fe_2O_3 nanoparticles-filled carbon nanotubes. *Chem. Commun.* **2010**, *46*, 8576–8578.

[14] Zhang, W.; Wu, X.; Hu, J.; Guo, Y.; Wan, L. Carbon coated Fe_3O_4 nanospindles as a superior anode material for lithium-ion batteries. *Adv. Funct. Mater.* **2008**, *18*, 3941–3946.

[15] Arico, A. S.; Bruce, P.; Scrosati, B.; Tarascon, J. M.; Van Schalkwijk, W. Nanostructured materials for advanced energy conversion and storage devices. *Nat. Mater.* **2005**, *4*, 366–377.

[16] Poizot, P.; Laruelle, S.; Grugeon, S.; Tarascon, J. M. Rationalization of the low-potential reactivity of 3d-metal-based inorganic compounds toward Li. *J. Electrochem. Soc.* **2002**, *149*, A1212–1217.

[17] Arora, P.; White, R. E.; Doyle, M. Capacity fade mechanisms and side reactions in lithium-ion batteries. *J. Electrochem. Soc.* **1998**, *145*, 3647–3667.

[18] Inagaki, M. Carbon coating for enhancing the functionalities of materials. *Carbon* **2012**, *50*, 3247–3266.

[19] Yang, S.; Sun, Y.; Chen, L.; Hernandez, Y.; Feng, X.; Müllen, K. Porous iron oxide ribbons grown on graphene for high-performance lithium storage. *Sci. Rep.* **2012**, *2,* 427–433.

[20] Li, H.; Zhou, H. Enhancing the performances of Li-ion batteries by carbon-coating: Present and future. *Chem. Commun.* **2012**, *48*, 1201–1217.

[21] Li, B.; Cao, H.; Shao, J.; Qu, M. Enhanced anode performances of the Fe_3O_4-carbon-rGO three dimensional composite in lithium ion batteries. *Chem. Commun.* **2011**, *47*, 10374–10376.

[22] Liu, H.; Wang, G.; Wang, J.; Wexler, D. Magnetite/carbon core–shell nanorods as anode materials for lithium-ion batteries. *Electrochem. Commun.* **2008**, *10*, 1879–1882.

[23] Muraliganth, T.; Vadivel Murugan, A.; Manthiram, A. Facile synthesis of carbon-decorated single-crystalline Fe_3O_4 nanowires and their application as high performance anode in lithium ion batteries. *Chem. Commun.* **2009**, 7360–7362.

[24] Lu, A. H.; Li, W. C.; Salabas, E. L.; Spliethoff, B.; Schüth, F. Low temperature catalytic pyrolysis for the synthesis of high surface area, nanostructured graphitic carbon. *Chem. Mater.* **2006**, *18*, 2086–2094.

[25] Wilcox, J. D.; Doeff, M. M.; Marcinek, M.; Kostecki, R. Factors influencing the quality of carbon coatings on $LiFePO_4$. *J. Electrochem. Soc.* **2007**, *154*, A389–395.

[26] L'vov, B. V. Mechanism of carbothermal reduction of iron, cobalt, nickel and copper oxides. *Thermochim. Acta* **2000**, *360*, 109–120.

[27] Li, Z.; Sun, Q.; Gao, M. Preparation of water-soluble magnetite nanocrystals from hydrated ferric salts in 2-pyrrolidone: Mechanism leading to Fe_3O_4. *Angew. Chem. Int. Edit.* **2005**, *44*, 123–126.

[28] Martha, S. K.; Grinblat, J.; Haik, O.; Zinigrad, E.; Drezen, T.; Miners, J. H.; Exnar, I.; Kay, A.; Markovsky, B.; Aurbach, D. $LiMn_{0.8}Fe_{0.2}PO_4$: An advanced cathode material for rechargeable lithium batteries. *Angew. Chem. Int. Edit.* **2009**, *48*, 8559–8563.

[29] Zhao, L.; Hu, Y. S.; Li, H.; Wang, Z.; Chen, L. Porous $Li_4Ti_5O_{12}$ coated with N-doped carbon from ionic liquids for Li-ion batteries. *Adv. Mater.* **2011**, *23*, 1385–1388.

[30] Zhang, W. M.; Hu, J. S.; Guo, Y. G.; Zheng, S. F.; Zhong, L. S.; Song, W. G.; Wan, L. J. Tin-nanoparticles encapsulated in elastic hollow carbon spheres for high-performance anode material in lithium-ion batteries. *Adv. Mater.* **2008**, *20*, 1160–1165.

[31] Lee, K. T.; Jung, Y. S.; Oh, S. M. Synthesis of tin-encapsulated spherical hollow carbon for anode material in lithium secondary batteries. *J. Am. Chem. Soc.* **2003**, *125*, 5652–5653.

[32] Zhou, J.; Song, H.; Chen, X.; Zhi, L.; Yang, S.; Huo, J.; Yang, W. Carbon-encapsulated metal oxide hollow nanoparticles and metal oxide hollow nanoparticles: A general synthesis strategy and its application to lithium-ion batteries. *Chem. Mater.* **2009**, *21*, 2935–2940.

[33] Yu, W. J.; Hou, P. X.; Li, F.; Liu, C. Improved electrochemical performance of Fe_2O_3 nanoparticles confined in carbon nanotubes. *J. Mater. Chem.* **2012**, *22*, 13756–13763.

[34] Fujii, T.; de Groot, F. M. F.; Sawatzky, G. A.; Voogt, F. C.; Hibma, T.; Okada, K. *In situ* XPS analysis of various iron oxide films gown by NO_2-assisted molecular-beam epitaxy. *Phys. Rev. B* **1999**, *59*, 3195–3202.

[35] Zhou, G.; Wang, D. W.; Li, F.; Zhang, L.; Li, N.; Wu, Z. S.; Wen, L.; Lu, G. Q.; Cheng, H. M. Graphene-wrapped Fe_3O_4 anode material with improved reversible capacity and cyclic stability for lithium ion batteries. *Chem. Mater.* **2010**, *22*, 5306–5313.

[36] Zhou, W.; Lin, L.; Wang, W.; Zhang, L.; Wu, Q.; Li, J.; Guo, L. Hierarchial mesoporous hematite with "electron-transport channels" and its improved performances in photocatalysis and lithium ion batteries. *J. Phys. Chem. C* **2011**, *115*, 7126–7133.

[37] Sun, B.; Horvat, J.; Kim, H. S.; Kim, W. S.; Ahn, J.; Wang, G. Synthesis of mesoporous α-Fe_2O_3 nanostructures for highly sensitive gas sensors and high capacity anode materials in lithium ion batteries. *J. Phys. Chem. C* **2010**, *114*, 18753–18761.

[38] Ma, Y.; Ji, G.; Lee, J. Y. Synthesis of mixed-conducting carbon coated porous γ-Fe_2O_3 microparticles and their properties for reversible lithiumi storage. *J. Mater. Chem.* **2011**, *21*, 13009–13014.

[39] Chou, S. L.; Wang, J. Z.; Wexler, D.; Konstantinov, K.; Zhong, C.; Liu, H. K.; Dou, S. X. High-surface-area γ-Fe_2O_3/carbon nanocomposite: One-step synthesis and its highly reversible and enhanced high-rate lithium storage properties. *J. Mater. Chem.* **2010**, *20*, 2092–2098.

[40] Wang, Z.; Luan, D.; Madhavi, S.; Li, C. M.; Lou, X. W. γ-Fe_2O_3 nanotubes with superior lithium storage capability. *Chem. Commun.* **2011**, *47*, 8061–8063.

[41] Wang, B.; Chen, J. S.; Wu, H. B.; Wang, Z.; Lou, X. W. Quasiemulsion-templated formation of α-Fe_2O_3 hollow spheres with enhanced lithium storage properties. *J. Am. Chem. Soc.* **2011**, *133*, 17146–17148.

[42] Wang, Z.; Luan, D.; Madhavi, S.; Hu, Y.; Lou, X. W. Assembling carbon-coated γ-Fe_2O_3 hollow nanohorns on the CNT backbone for superior lithium storage capability. *Energ. Environ. Sci.* **2012**, *5*, 5252–5256.

[43] Kang, E.; Jung, Y. S.; Cavanagh, A. S.; Kim, G. H.; George, S. M.; Dillon, A. C.; Kim, J. K.; Lee, J. Fe_3O_4 nanoparticles confined in mesocellular carbon foam for high performance anode materials for lithium-ion batteries. *Adv. Funct. Mater.* **2011**, *21*, 2430–2438.

[44] Zhou, G.; Wang, D. W.; Hou, P. X.; Li, W.; Li, N.; Liu, C.; Li, F.; Cheng, H. M. A nanosized Fe_2O_3 decorated single-walled carbon nanotube membrane as a high-performance flexible anode for lithium ion batteries. *J. Mater. Chem.* **2012**, *22*, 17942–17946.

[45] Han, F.; Li, W. C.; Li, M. R.; Lu, A. H. Fabrication of superior-performance SnO_2@C composites for lithium-ion anodes using tubular mesoporous carbon with thin carbon walls and high pore volume. *J. Mater. Chem.* **2012**, *22*, 9645–9651.